ANNULAR SEAL BULK-FLOW MODEL FOR THE TRANSITION TO TURBULENCE REGIME: NUMERICAL PRODUCTION

Nicole Zirkelback

Dr. San Andres

May 1995

TRC-SEAL-3-95

Texas A&M University
Mechanical Engineering Department

Annular Seal Bulk-Flow Model for the Transition to Turbulence Regime: Numerical Predictions

by

Nicole Zirkelback
undergraduate research assistant

A Research Progress Report
to the
Turbomachinery Research Consortium

May 1995

TRC Project:
A Flow Model for Annular Seals Operating
in the Transition Regime to Turbulence
Principal Investigator: Dr. Luis San Andres, Associate Professor

TABLE OF CONTENTS

NOMENCLATURE

c_*	seal nominal clearance [m]
$C_{\alpha\beta}$	damping force coefficients; $\alpha, \beta = X,Y$ [N·s/m]
D	rotor diameter [m]
f_r, f_s	friction factors for bulk-flow model; see equation (A.1)
f_r^*, f_s^*	Moody's turbulent flow friction factors at rotor and stator surfaces; see eqn (11)
h	dimensionless film thickness; $h = H/c_* = 1 + \varepsilon_X \cos\theta + \varepsilon_Y \sin\theta$
h_X, h_Y	$\cos\theta, \sin\theta$
k_x, k_y	$\frac{1}{2}(k_r + k_s)$, dimensionless shear parameters in axial and circumferential directions
k_r, k_s	$f_r R_r, f_s R_s$, shear parameters at rotor and stator surfaces
$K_{\alpha\beta}$	stiffness force coefficients; $\alpha, \beta = X,Y$ [N/m]
$M_{\alpha\beta}$	inertia force coefficients; $\alpha, \beta = X,Y$ [kg]
P	fluid pressure [Pa]
P_s, P_a	external supply and discharge pressures [Pa]
ΔP	$(P_s - P_a)$; pressure drop across seal [Pa]
p	$(P - P_a)/\Delta P$, dimensionless pressure
p_e	$(P_e - P_a)/\Delta P$, dimensionless pressure at seal entrance
p_X, p_Y	dimensionless dynamic pressures for perturbations in the X,Y directions
R	rotor radius [m]
Re	$\rho_* \Omega c_* R/\mu_*$, nominal circumferential flow Reynolds number
Re_p	$\rho_* c_*^3 \Delta P/\mu_*^2 R$, nominal pressure flow Reynolds number
Re_p^*	$\mathrm{Re}_p(c_*/R)$, modified pressure flow Reynolds number
Re_S	$\rho_* \omega c_*^2/\mu_*$, squeeze film Reynolds number
R_r	$(\rho/\mu)H[(U - \Omega R)^2 + V^2]^{1/2}$, Reynolds number relative to rotor surface
R_s	$(\rho/\mu)H[U + V]^{1/2}$, Reynolds number relative to stator surface
r_s, r_r	mean surface roughness at stator and rotor [m]
U_*	$\Delta P c_*^2/\mu_* R$, characteristic fluid velocity [m/s]

u	U/U_*, dimensionless circumferential bulk-flow velocity
v	V/U_*, dimensionless axial bulk-flow velocity
$\{X, Y\}$	inertial coordinate system
$\{x,y\}$	coordinate system on seal plane; $\{\bar{x},\bar{y}\} = \{x/R, y/R\}$
α	$(1 + \xi)$, ξ: empirical entrance loss factor
β	$U\|_{y=0}/\Omega R$, entrance swirl factor
γ	first order perturbed shear coefficients given in eqns. (10) and (15).
ε_X, ε_Y	e_X/c^*, e_Y/c^*, dimensionless rotor eccentricities in X, Y directions
$\Delta\varepsilon_X$, $\Delta\varepsilon_Y$	dimensionless perturbed eccentricities
Λ	$\Omega R/U_*$, characteristic dimensionless rotor velocity
μ, μ_*, $\bar{\mu}$	fluid absolute viscosity [Pa·s], characteristic viscosity, μ/μ_*
ρ, ρ_*, $\bar{\rho}$	fluid density [kg/m^3], characteristic density, ρ/ρ_*
σ	$u_*\omega R^2/c_*^2\Delta P$, whirl frequency parameter
τ	ωt, dimensionless time coordinate
Ω	angular velocity of rotor (1/s)
ω	excitation or whirl frequency (1/s)

Subscripts

e	entrance
0	zeroth-order solution
r	rotor
s	stator
α, β	first order perturbations in X, Y directions
*	characteristic value

Executive Summary

An analysis and computational program for the prediction of the seal force response in the transition flow regime for annular seals are presented. The laminar friction factor line and Moody's turbulent friction factor lines are connected with a cubic polynomial in the transition regime from laminar to fully developed turbulent flow. This curve fit provides a continuous shift in the friction factor through the transition flow regime to turbulence. The modifications are incorporated into a seal program described in San Andres (1991). The force coefficients for this analysis compared with those for the traditional analysis are given for varying seal clearances. Predicted results indicate an elimination of the discontinuities in the force coefficients calculated in conventional analyses for annular seals.

Introduction

Annular seals are used to block secondary flows in turbomachinery. In pump applications, seals operating as neck ring or interstage seals lessen leakage of the process fluid from higher pressures to lower pressures. Black (1969) first described the effect of annular seals on rotordynamic behavior. His conclusion that seals are a primary influence on the behavior of high-performance turbomachinery has been the inspiration for many innovations and advances in the study of annular seals. Unlike fluid film bearings, high pressure gradients, large clearance to radius ratios, and low viscosity process fluids typical in annular seals characterize the flow as turbulent in most cases. Black, et al.

Childs (1983) introduced an analysis which predicts the dynamic force response in annular seals. For fully developed turbulent flows in both the axial and circumferential directions, linear zeroth- and first-order perturbation solutions determine the static and dynamic force characteristics of an annular seal. Childs' model employs Hirs' turbulent bulk flow theory (Hirs, 1973), where wall shear stresses are represented as a combination of shear and pressure flow contributions. The friction factor developed in the flow is said to be dependent on two constants which depend solely on the Reynolds number relative to the rotor and stator surfaces.

Von Pragenau (1982) first analyzed the use of rough stators and smooth rotors in annular seals. His findings indicate that intentionally roughened stators and smooth rotors reduce undesired cross-coupled stiffness effects and improve seal stability. By using a surface roughness model, Childs (1985) found that tapered seals decrease leakage while providing an overall increase in damping. The need for an analysis adequate to model macroscopically rough surfaces led to the realization that Hirs' equation lacks the physical insight necessary to represent these situations. Moody's friction factor, adapted from the Moody diagram for pipe flow, accounts for both flow Reynolds number and surface roughness, as introduced by Nelson and Nguyen (1987). These authors present comparisons with Hirs' friction factor model. For smooth seals Hirs' equation and Moody's equation yielded nearly identical results; however, calculations based on Moody's model deviated significantly for roughened seals, predicting higher direct and cross-coupled stiffnesses and smaller cross-coupled damping coefficients. Historically, Hirs' based models underpredict direct stiffness compared to measured values, and this

departure increases with increasing surface roughness. Thus, the results from Moody's equation indicate an improvement in the prediction of rotordynamic coefficients.

Until now, annular seals have been studied in the turbulent regime due to high axial pressure gradients and large clearance to radius ratios typical of liquid/gas applications. However, annular seals used in the petrochemical industry typically operate with high viscosity fluids and relatively low shaft speeds (1,800 to 3,600 RPM). Increased clearances due to normal or unexpected wear cause seals that would normally function in the laminar regime to operate in the transition regime to turbulence. Shapiro, et al (1991) have introduced an analytical formula to predict analyzes the performance of annular seals in the laminar, transition, and turbulent flow regimes. However, their model neglects fluid inertia effects.

San Andres (1991) presents a more detailed analysis for seals which includes the effects of fluid inertia and variable fluid properties on dynamic force response of annular seals. The computational program described in his analysis includes computations of the rotordynamic force coefficients in both the laminar and turbulent flow regimes. Predictions from the model compare well with other analyses and with available experimental results. However, the lack of a sound analysis in the transition flow regime leads to discontinuities in the predictions of the dynamic force coefficients, since the flow is either laminar or fully developed turbulent flow with a sharp discontinuity in the friction factor.

The objective of this report is to provide a more accurate tool for the state-of-the-art design of annular seals. More specifically, the equations which govern the flow within the annulus of the seal are modified to obtain more acceptable results by introducing a universal friction factor equation valid for all regimes. These modifications for the transition regime to turbulence are incorporated in the computer program developed by San Andres (1991). The results obtained from the modified code are then compared to the traditional analysis across the transition flow regime.

ANALYSIS

Figure 1 shows an annular seal operating at an eccentric position. (e_X, e_Y) describe the translational displacement of the shaft from its centered position. The shaft rotates at angular speed Ω, and the fluid is confined to the space in the annulus between rotor and stator where H is the seal clearance. A pressure drop at the entrance of the seal due to fluid inertia effects greatly influences the performance of the seal.

In the annulus of the seal, the continuity and momentum equations for isothermal flow conditions are given for a variable property fluid as (San Andres, 1991):

$$\frac{\partial}{\partial x}(\rho HU)+\frac{\partial}{\partial y}(\rho HV)+\frac{\partial}{\partial t}(\rho H)=0$$

$$-H\frac{\partial P}{\partial x}=\frac{\mu}{H}\left(k_x U-k_r\frac{\Omega R}{2}\right)+\left\{\frac{\partial}{\partial t}(\rho HU)+\frac{\partial}{\partial x}\left(\rho HU^2\right)+\frac{\partial}{\partial y}(\rho HUV)\right\} \qquad \textbf{(1)}$$

$$-H\frac{\partial P}{\partial y}=\frac{\mu}{H}k_y V+\left\{\frac{\partial}{\partial t}(\rho HV)+\frac{\partial}{\partial x}(\rho HUV)+\frac{\partial}{\partial y}\left(\rho HV^2\right)\right\}$$

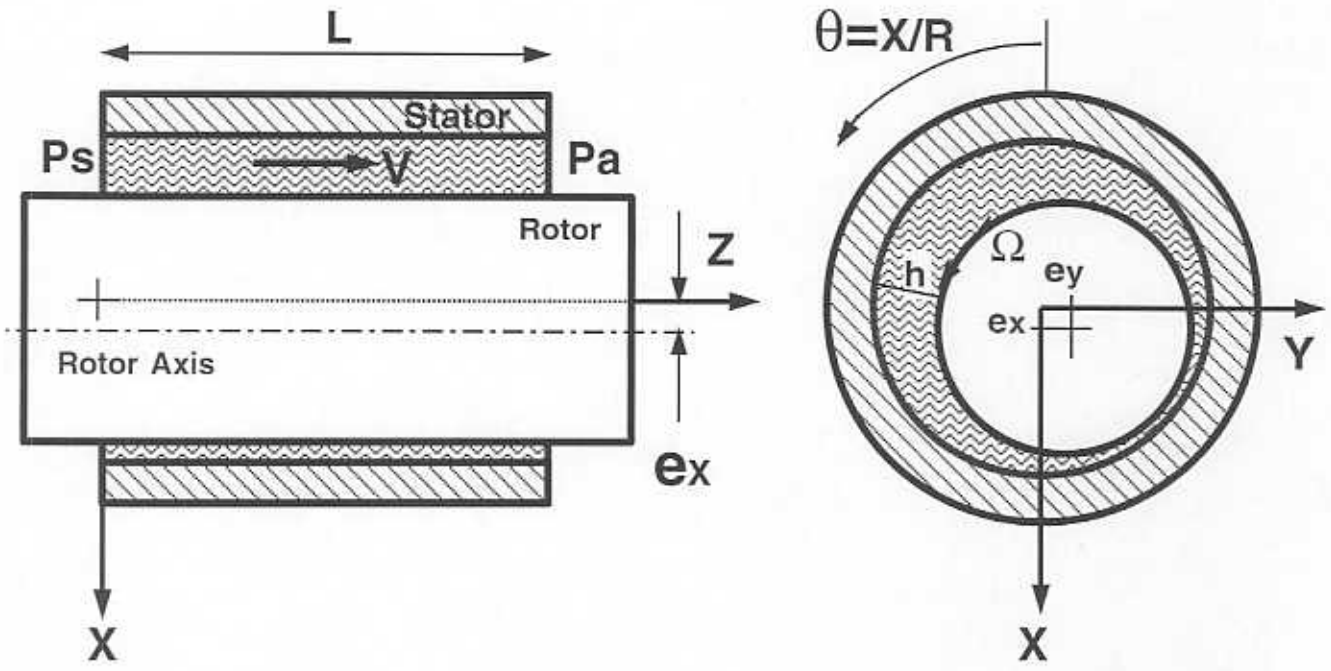

Figure 1. Geometrical Description of Annular Pressure Seal

$$\{0 \le x \le 2\pi R,\ 0 \le y \le L\}$$

Refer to the nomenclature for a proper definition of all variables. Consider the rotor to describe small motions of amplitude (Δe_X, Δe_Y) at frequency ω about an equilibrium position (e_{X0}, e_{Y0}). Then the film thickness is given in dimensionless form as

$$h = h_0 + (\Delta\varepsilon_X H_X + \Delta\varepsilon_Y H_Y)e^{i\omega t} \tag{2}$$

where

$$h_0 = H/C_* = 1 + \varepsilon_{X0}\cos\theta + \varepsilon_{Y0}\sin\theta \ ; \qquad h_X = \cos\theta;\ h_Y = \sin\theta$$

For small amplitude motions, the flow variables are also given in dimensionless form by

$$\begin{aligned}
p &= p_0 + e^{i\tau}(\Delta\varepsilon_X p_X + \Delta\varepsilon_Y p_Y) \\
u &= u_0 + e^{i\tau}(\Delta\varepsilon_X u_X + \Delta\varepsilon_Y u_Y) \\
v &= v_0 + e^{i\tau}(\Delta\varepsilon_X v_X + \Delta\varepsilon_Y v_Y) \\
\overline{\rho} &= \overline{\rho}_0 + e^{i\tau}(\Delta\varepsilon_X \overline{\rho}_X + \Delta\varepsilon_Y \overline{\rho}_Y) = \overline{\rho}(p) \\
\mu &= \mu_0 + e^{i\tau}(\Delta\varepsilon_X \mu_X + \Delta\varepsilon_Y \mu_Y) = \mu(p); \qquad \mathbf{i} = \sqrt{-1} \\
k_j &= k_{j0} + e^{i\tau}(\Delta\varepsilon_X k_{jX} + \Delta\varepsilon_Y k_{jY}), \qquad j = X, Y, r, s
\end{aligned} \tag{3}$$

Substituting these into the governing equations gives the *zeroth-order dimensionless equations* (San Andres, 1991):

$$\frac{\partial}{\partial x}(\overline{\rho}_0 h_0 u_0) + \frac{\partial}{\partial y}(\overline{\rho}_0 h_0 v_0) = 0$$

$$\begin{aligned}
-h_0\frac{\partial p_0}{\partial x} &= \frac{\overline{\mu}_0}{h_0}\left(k_{x0}u_0 - k_{r0}\frac{\Lambda}{2}\right) + \mathrm{Re}_p^*\left\{\frac{\partial}{\partial x}(\overline{\rho}_0 h_0 u_0^2) + \frac{\partial}{\partial y}(\overline{\rho}_0 h_0 u_0 v_0)\right\} \\
-h_0\frac{\partial p_0}{\partial y} &= \frac{\overline{\mu}_0}{h_0}k_{y0}v_0 + \mathrm{Re}_p^*\left\{\frac{\partial}{\partial x}(\overline{\rho}_0 h_0 u_0 v_0) + \frac{\partial}{\partial y}(\overline{\rho}_0 h_0 v_0^2)\right\}
\end{aligned} \tag{4}$$

$$\left\{0 \le \bar{x} \le 2\pi,\ 0 < \bar{y} < \tfrac{L}{R}\right\}$$

The entrance pressure and circumferential velocity are prescribed as

$$p_{e0}\big|_{\bar{y}=0} = 1 - \frac{\alpha}{2}\bar{\rho}_0 v_0^2\big|_{\bar{y}=0}\ ; \qquad u_0\big|_{\bar{y}=0} = \beta\Lambda \tag{5.a}$$

while the discharge pressure is set to

$$p_0\left(\bar{y} = \tfrac{L}{R}\right) = 0 \tag{5.b}$$

The *first-order dimensionless equations* are given by (San Andres, 1991):

$$\frac{\partial}{\partial \bar{x}}\left(\bar{\rho}_0 u_\alpha h_0 + \bar{\rho}_0 u_0 h_\alpha + \bar{\rho}_\alpha u_0 h_0\right) + \frac{\partial}{\partial \bar{y}}\left(\bar{\rho}_0 v_\alpha h_0 + \bar{\rho}_0 v_0 h_\alpha + \bar{\rho}_\alpha v_0 h_0\right) = -\mathbf{i}\sigma\left(\bar{\rho}_0 h_\alpha + \bar{\rho}_\alpha h_0\right)$$

$$\begin{aligned}
-h_0\frac{\partial p_0}{\partial \bar{x}} &= \mathbf{i}\bar{\rho}_0 h_0\,\mathrm{Re}_s\,u_\alpha + \gamma_{xx}u_\alpha + \gamma_{xy}v_\alpha + \gamma_{xh}h_\alpha + \gamma_{x\rho}\bar{\rho}_\alpha + \gamma_{x\mu}\bar{\mu}_\alpha \\
&\quad + \mathrm{Re}_p^*\left\{\frac{\partial}{\partial \bar{x}}\left(\bar{\rho}_0 h_0 u_0 u_\alpha\right) + \frac{\partial}{\partial \bar{y}}\left(\bar{\rho}_0 h_0 v_0 u_\alpha\right) + \rho_0 h_0\left[u_\alpha\frac{\partial u_0}{\partial \bar{x}} + v_\alpha\frac{\partial u_0}{\partial \bar{y}}\right]\right\} \\
-h_0\frac{\partial p_0}{\partial \bar{y}} &= \mathbf{i}\bar{\rho}_0 h_0\,\mathrm{Re}_s\,v_\alpha + \gamma_{yy}v_\alpha + \gamma_{yx}u_\alpha + \gamma_{yh}h_\alpha + \gamma_{y\rho}\bar{\rho}_\alpha + \gamma_{y\mu}\bar{\mu}_\alpha \\
&\quad + \mathrm{Re}_p^*\left\{\frac{\partial}{\partial \bar{x}}\left(\bar{\rho}_0 h_0 u_0 v_\alpha\right) + \frac{\partial}{\partial \bar{y}}\left(\bar{\rho}_0 h_0 v_0 v_\alpha\right) + \rho_0 h_0\left[u_\alpha\frac{\partial v_0}{\partial \bar{x}} + v_\alpha\frac{\partial v_0}{\partial \bar{y}}\right]\right\}
\end{aligned} \tag{6}$$

where $\alpha = X, Y$ corresponds to rotor perturbations in the X and Y directions, respectively.

The boundary conditions for the perturbed fields are:

$$\begin{aligned}
&p_\alpha\big|_{\bar{y}=0} = \tfrac{\alpha}{2}\left(\bar{\rho}_\alpha v_0^2 + 2\bar{\rho}_0 v_0 v_\alpha\right)\ ; \qquad u_\alpha\big|_{\bar{y}=0} = 0,\ \text{and} \\
&p_\alpha\big|_{\bar{y}=L/R} = 0
\end{aligned} \tag{7}$$

The zeroth- and first-order dimensionless equations describe the equilibrium rotor position and perturbed dynamic motions, respectively. The perturbed shear coefficients

found in the first-order equations (γ_{xx}, γ_{xy}, γ_{xh}, etc.) arise from the perturbation of the shear coefficients k_x, k_y, etc. The general form of the perturbed shear coefficients is given by the following relationships:

$$\gamma_{yh} = \left(-2\frac{k_y}{h} + \frac{\partial k_y}{\partial h} \right)_0 \frac{\overline{\mu}_0 v_0}{h_0}$$

$$\gamma_{yy} = \left(\frac{k_y}{v} + \frac{\partial k_y}{\partial v} \right)_0 \frac{\overline{\mu}_0 v_0}{h_0}$$

$$\gamma_{yx} = \left(\frac{\partial k_y}{\partial u} \right)_0 \frac{\overline{\mu}_0 v_0}{h_0} \qquad \textbf{(8.a)}$$

$$\gamma_{y\mu} = \left(k_y + \frac{\partial k_y}{\partial \overline{\mu}} \overline{\mu} \right)_0 \frac{v_0}{h_0}$$

$$\gamma_{y\rho} = \left(-\frac{k_y}{\overline{\rho}} + \frac{\partial k_y}{\partial \overline{\rho}} \right)_0 \frac{\overline{\mu}_0 v_0}{h_0} - \frac{h_0}{\overline{\rho}_0} \frac{\partial p_0}{\partial y}$$

$$\gamma_{xh} = \left(-2\frac{k_x}{h} + \frac{\partial k_x}{\partial h} \right)_0 \frac{\overline{\mu}_0 u_0}{h_0} + \left(2\frac{k_r}{h} - \frac{\partial k_r}{\partial h} \right)_0 \frac{\overline{\mu}_0 \Lambda}{2h_0}$$

$$\gamma_{xx} = \left(\frac{k_x}{u} + \frac{\partial k_x}{\partial u} \right)_0 \frac{\overline{\mu}_0 u_0}{h_0} + \left(-\frac{\partial k_r}{\partial u} \right)_0 \frac{\overline{\mu}_0 \Lambda}{2h_0}$$

$$\gamma_{xy} = \left(\frac{\partial k_x}{\partial v} u - \frac{\partial k_r}{\partial v} \frac{\Lambda}{2} \right)_0 \frac{\overline{\mu}_0}{h_0} \qquad \textbf{(8.b)}$$

$$\gamma_{x\mu} = \left(k_x + \frac{\partial k_x}{\partial \overline{\mu}} \overline{\mu} \right)_0 \frac{u_0}{h_0} - \left(k_J + \frac{\partial k_r}{\partial \overline{\mu}} \overline{\mu} \right)_0 \frac{\Lambda}{2h_0}$$

$$\gamma_{x\rho} = \left(-\frac{k_x}{\overline{\rho}} + \frac{\partial k_x}{\partial \overline{\rho}} \right)_0 \frac{\overline{\mu}_0 u_0}{h_0} - \left(-\frac{k_r}{\overline{\rho}} + \frac{\partial k_r}{\partial \overline{\rho}} \right)_0 \frac{\overline{\mu}_0 \Lambda}{2h_0} - \frac{h_0}{\overline{\rho}_0} \frac{\partial p_0}{\partial x}$$

where $(k_s, k_s) = \left(\frac{k_r + k_s}{2}\right)$.

In general, the shear coefficients at the rotor and stator surfaces are described by the relations:

$$k_{r,s} = f_{r,s} \cdot R_{r,s} \tag{9}$$

For Reynolds numbers $R_{r,s} \leq 1000$ (laminar flow), the shear coefficients are $k_r = k_s = 12$. In this regime, the friction factor is just defined as

$$f_{r,s} = \frac{12}{R_{r,s}} \tag{10}$$

For turbulent flow ($R_{r,s} \geq 3000$), the friction factor presently used corresponds to the Moody equation presented by Nelson and Nguyen (1987). That is

$$f^*_{r,s} = a_M \left[1 + \left\{ c_M \left(\frac{r_{r,s}}{H} \right) + \frac{b_M}{R_{r,s}} \right\}^{e_M} \right] \tag{11}$$

where $a_M = 0.001375$, $b_M = 5 \times 10^5$, $c_M = 10^4$, and $e_M = 1/3.0$.

Previous analyses have used the friction factor for turbulent flow starting at Reynolds number of 1,000. Figure 2 shows Moody's friction factor versus Reynolds number for increasing values of surface roughness. As shown in the diagram, transition from laminar to turbulent occurs at Reynolds numbers between 1,000 to 3,000. For simplicity, previous analyses extended the turbulent friction factor line through the transition regime until intersection with the laminar friction factor line. To obtain a more physically acceptable prediction, Shapiro et al. (1991) proposed a curve fit to the Moody diagram connecting laminar and turbulent friction factor lines in the transition regime.

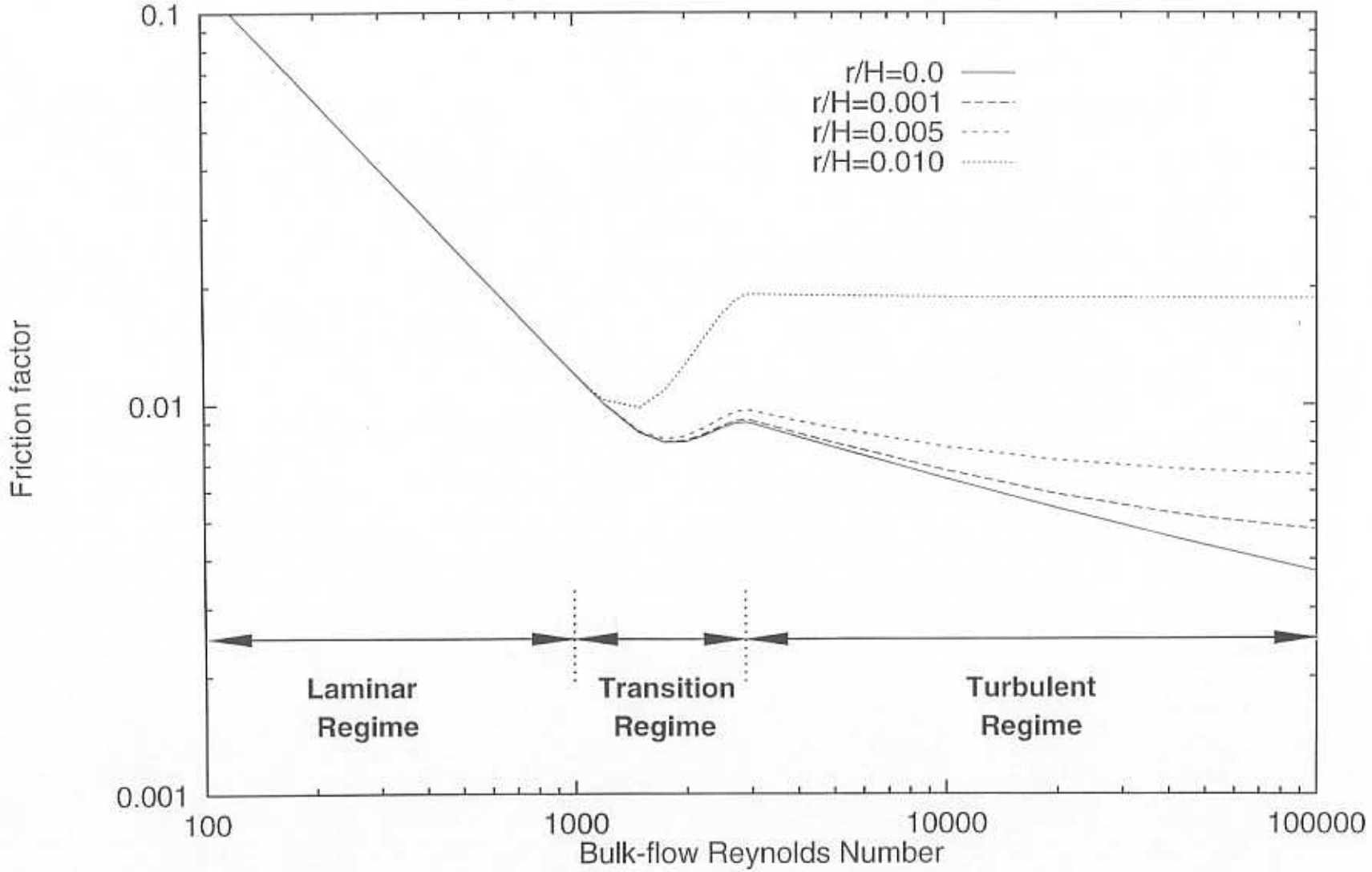

Figure 2. Friction factor diagram for various surface roughness ratios.

Using a cubic curve fit which most resembles available experimental data, the relation proposed is

$$f_{r,s} = \frac{12}{R_{r,s}}\left(1 - 3\xi_{r,s}^2 + 2\xi_{r,s}^3\right) + f_{r,s}^*\left(3\xi_{r,s}^2 - 2\xi_{r,s}^3\right) \tag{12}$$

$$\text{where } \xi_{r,s} = \frac{R_{r,s} - A_1}{A_2}, \quad A_1 = 1000, \quad A_2 = 2000, \tag{13}$$

and $f_{r,s}^*$ is Moody's friction factor given by eqn. (11). The shear factors versus Reynolds number is shown in Figure 3. A previously abrupt change at a Reynolds number of 1000 is now replaced with a gradual curve in the transition regime. Defining the following equations:

$$t_{1r,s} = \begin{cases} 0 & R_{r,s} \le 1000 \\ \dfrac{6\xi_{r,s}\left(1 - \xi_{r,s}\right)\left(k_{r,s}^* - 12\right)}{A_2} & 1000 < R_{r,s} < 3000 \\ 0 & R_{r,s} \ge 3000 \end{cases}$$

$$t_{2r,s} = \begin{cases} 0 & R_{r,s} \le 1000 \\ \xi_{r,s}^2\left(3 - 2\xi_{r,s}\right) & 1000 < R_{r,s} < 3000 \\ 1 & R_{r,s} \ge 3000 \end{cases} \tag{14}$$

and substituting the appropriate expressions into the general form of the perturbed shear coefficients gives the following lengthy algebraic expressions:

Perturbed Shear Coefficients (15)	
γ_{yh}	$\frac{\overline{\mu}_0 v_0}{h_0^2}\left[-4k_y + t_{1r}R_r + t_{1s}R_s + t_{2r}\left(2C_{cr} + k_r^*\right) + t_{2s}\left(2C_{cs} + k_s^*\right)\right]$
γ_{yy}	$\overline{\mu}_0\left\{\frac{k_y}{h} + \frac{v^2\left(\mathrm{Re}_p\frac{\overline{\rho}}{\overline{\mu}}\right)^2 h}{2}\left(\frac{t_{1r}}{R_r} + \frac{t_{1s}}{R_s}\right) + t_{2r}f_{r1}v^2 + t_{2s}f_{s1}v^2\right\}_0$
γ_{yx}	$\overline{\mu}_0\left\{\frac{v\left(\mathrm{Re}_p\frac{\overline{\rho}}{\overline{\mu}}\right)^2 h}{2}\left(\frac{t_{1r}(u-\Lambda)}{R_r} + \frac{t_{1s}u}{R_s}\right) + t_{2r}f_{r1}v(u-\Lambda) + t_{2s}f_{s1}uv\right\}_0$
γ_{yu}	$\frac{V}{2h_0}\left[2k_y + t_{1r}R_r + t_{1s}R_s - t_{2r}\left(k_r^* + \gamma_r b_M\right) - t_{2s}\left(k_s^* + \gamma_s b_M\right)\right]$
γ_{yp}	$\frac{\overline{\mu}_0 v_0}{2h_0\overline{\rho}_0}\left[-2k_y + t_{1r}R_r + t_{1s}R_s + t_{2r}\left(k_r^* + \gamma_r b_M\right) + t_{2s}\left(k_s^* + \gamma_s b_M\right)\right] - \frac{h_0}{\overline{\rho}_0}\frac{\partial p_0}{\partial y}$
γ_{xh}	$\frac{\overline{\mu}_0}{h_0^2}\left\{-2k_x u + k_r\Lambda + \frac{t_{1r}R_r(u-\Lambda)}{2} + \frac{t_{1s}R_s u}{2} + t_{2r}(u-\Lambda)\left[C_{cr} + \frac{k_r^*}{2}\right] + t_{2s}u\left[C_{cs} + \frac{k_s^*}{2}\right]\right\}_0$
γ_{xx}	$\overline{\mu}_0\left\{\frac{k_x}{h} + \frac{\left(\mathrm{Re}_p\frac{\overline{\rho}}{\overline{\mu}}\right)^2 h}{2}\left(\frac{t_{1r}(u-\Lambda)^2}{R_r} + \frac{t_{1s}u^2}{R_s}\right) + t_{2r}f_{r1}(u-\Lambda)^2 + t_{2s}f_{s1}u^2\right\}_0$
γ_{xy}	$\overline{\mu}_0\left\{\frac{v\left(\mathrm{Re}_p\frac{\overline{\rho}}{\overline{\mu}}\right)^2 h}{2}\left(\frac{t_{1r}(u-\Lambda)}{R_r} + \frac{t_{1s}u}{R_s}\right) + t_{2r}f_{r1}v(u-\Lambda) + t_{2s}f_{s1}vu\right\}_0$
γ_{xu}	$\frac{1}{2h_0}\left[2k_x u - k_r^*\Lambda + t_{1r}R_r(u-\Lambda) + t_{1s}R_s u - t_{2r}(u-\Lambda)\left(k_r^* + \gamma_r b_M\right) - t_{2s}u\left(k_s^* + \gamma_s b_M\right)\right]_0$
γ_{xp}	$\frac{\overline{\mu}_0}{2h_0\overline{\rho}_0}\left[-2k_x + k_r^*\Lambda + t_{1r}R_r(u-\Lambda) + t_{1s}R_s u + t_{2r}(u-\Lambda)\left(k_r^* + \gamma_r b_M\right) + t_{2s}u\left(k_s^* + \gamma_s b_M\right)\right]_0 - \frac{h_0}{\overline{\rho}_0}\frac{\partial p_0}{\partial x}$

where

$C_{cr} = \tfrac{1}{2}\left(\frac{R_r c_M r_r}{c_* h_0} + b_M\right)\gamma_r$	$C_{cs} = \tfrac{1}{2}\left(\frac{R_s c_M r_s}{c_* h_0} + b_M\right)\gamma_s$
$f_{r1} = \frac{\left(\mathrm{Re}_p\frac{\overline{\rho}}{\overline{\mu}}\right)^2 h_0}{2R_r}\left(f_r^* + \frac{\gamma_r b_M}{R_r}\right)$	$f_{s1} = \frac{\left(\mathrm{Re}_p\frac{\overline{\rho}}{\overline{\mu}}\right)^2 h_0}{2R_s}\left(f_s^* + \frac{\gamma_s b_M}{R_s}\right)$
$\gamma_r = \frac{-a_M \cdot e_M}{\left[f_r^*/a_M - 1\right]^{\left(\gamma/e_M - 1\right)}}$	$\gamma_s = \frac{-a_M \cdot e_M}{\left[f_s^*/a_M - 1\right]^{\left(\gamma/e_M - 1\right)}}$

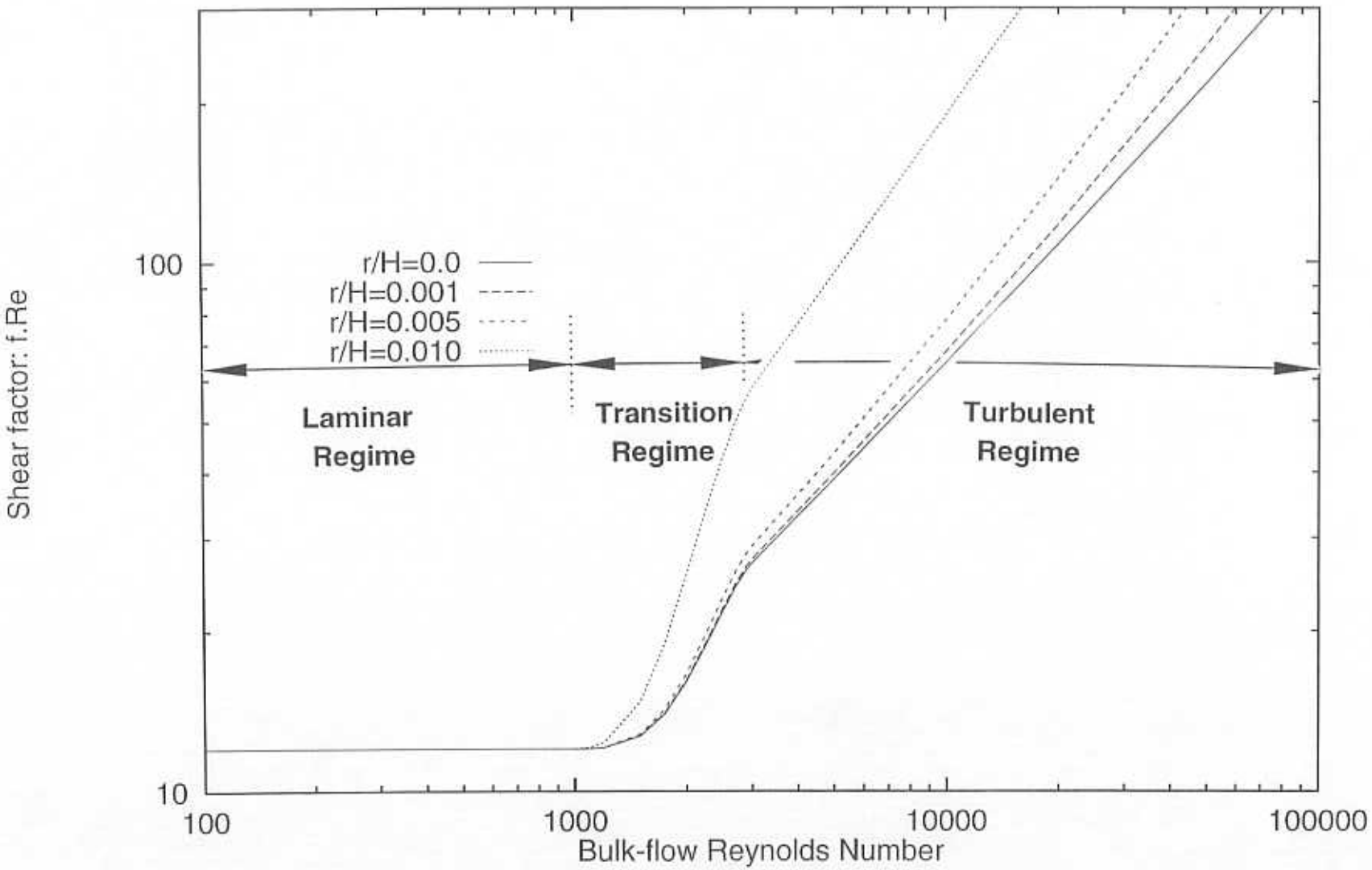

Figure 3. Shear factor vs. Reynolds number for increasing surface roughness ratios

These coefficients adjust the first-order equation for a more accurate prediction for the dynamic force coefficients in the transition regime. The formulation provided applies to the laminar, transition, and fully developed turbulent regimes.

PROCEDURE

The equations for the perturbed shear coefficients in the transition regime were incorporated into the seal program described in detail by San Andres (1991). Test cases were run using fluid properties representative of a process fluid (light oil) in the petrochemical industry. The following seal geometric parameters and operating conditions were used.

$$P_s - P_a = 35 \text{ bars}$$

$$L = 0.0508 \text{ m} \qquad D = 0.1524 \text{ m}$$

$$\omega = 3000 \text{ RPM } (314.16 \ {}^{\text{rad}}/_{\text{s}})$$

$$\rho = 900 \ {}^{\text{kg}}/_{\text{m}^3}$$

$$\mu = 13 \times 10^{-3} \ {}^{\text{N-s}}/_{\text{m}^2}$$

$$\xi = 0.1$$

$$\varepsilon_{X0} = \varepsilon_{Y0} = 0$$

(centered condition, smooth rotor & smooth stator)

In these calculations, the seal clearance was varied from 190 μm to 900 μm with a nominal clearance of 381 μm. At the nominal clearance, the circumferential Reynolds number ($\text{Re}_c = \rho \cdot \Omega Rc / \mu \cdot$) is 631.3 and the axial flow Reynolds number ($\rho \cdot Vc \cdot / \mu \cdot = {}^{\dot{m}}/_{\pi D \mu}$) is 1193.2. The use of these particular range of clearances represents one of two

cases due to wear: 1) a seal initially designed to perform in the laminar flow regime actually operates in the transition flow regime; or 2) a seal that is designed to work in the transition flow regime actually operates in the turbulent flow regime.

RESULTS

Generally, discontinuities that exist at the beginning of the transition regime for the conventional analysis are eliminated with the improved analysis. Figure 4 shows the seal flow rate to increase with the seal clearance. Because the friction factor in the transition regime for the modified case is lower than the traditionally used friction factor, the leakage in the transition regime is predicted to be higher. Figure 5 shows the flow Reynolds number (R_z) and circumferential Reynolds number against the seal clearance. The circumferential Reynolds number increases linearly with clearance; however, the total Reynolds number increases slightly for the improved model over the conventional model. The fact that flow Reynolds number and circumferential Reynolds numbers are nearly the same at small clearances indicates that shear flow governs the flow in the seal. At large seal clearances, the flow within the seal is more dominated by pressure driven flow shown by the large difference between the two Reynolds numbers.

Figure 6 shows that the drag torque is expected to continue decreasing from the laminar flow regime to the onset of the transition flow regime. Minimum torque is obtained at the onset of the transition regime and then rapidly increases into the turbulent flow regime.

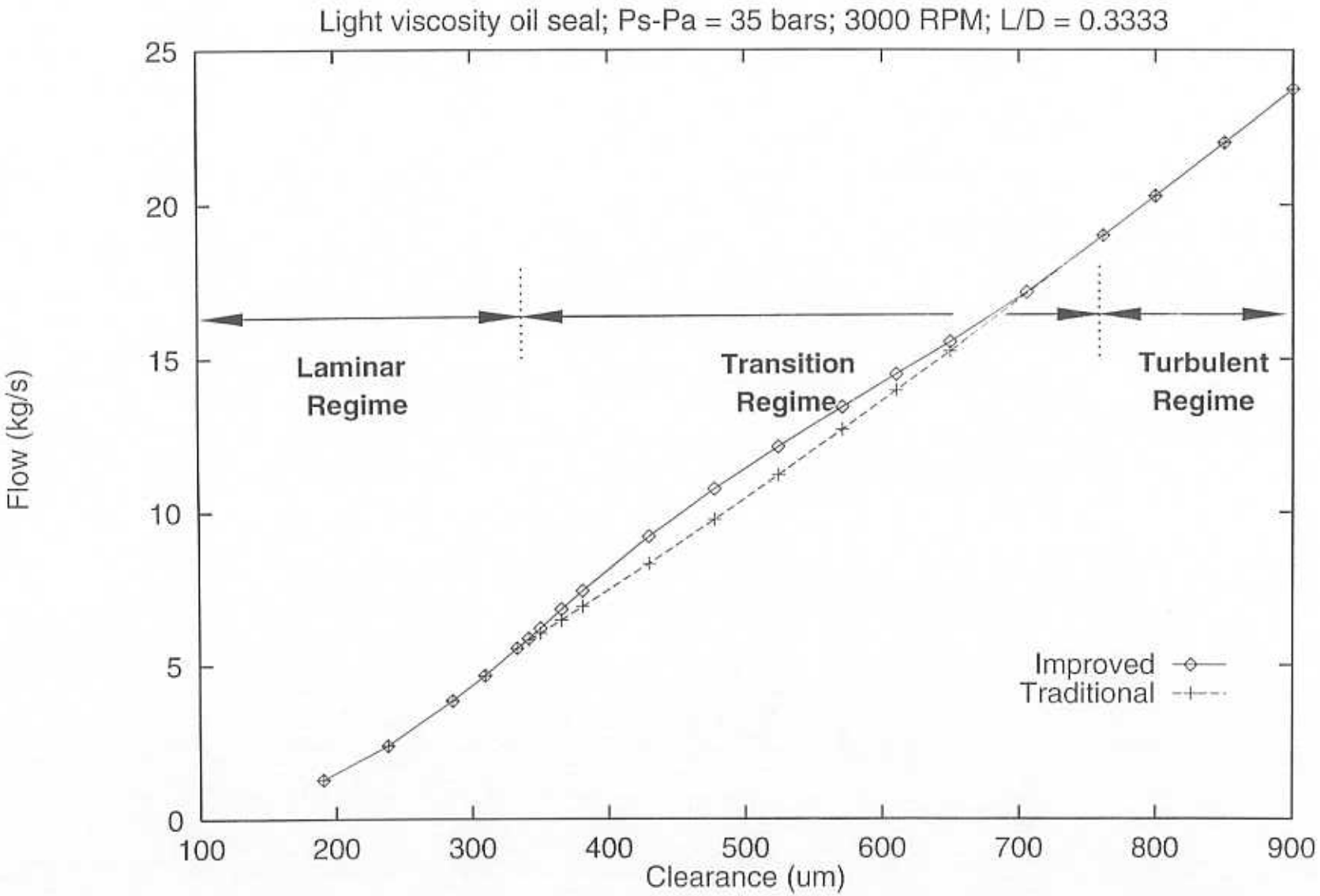

Figure 4. Seal flow rate vs. Operating clearance

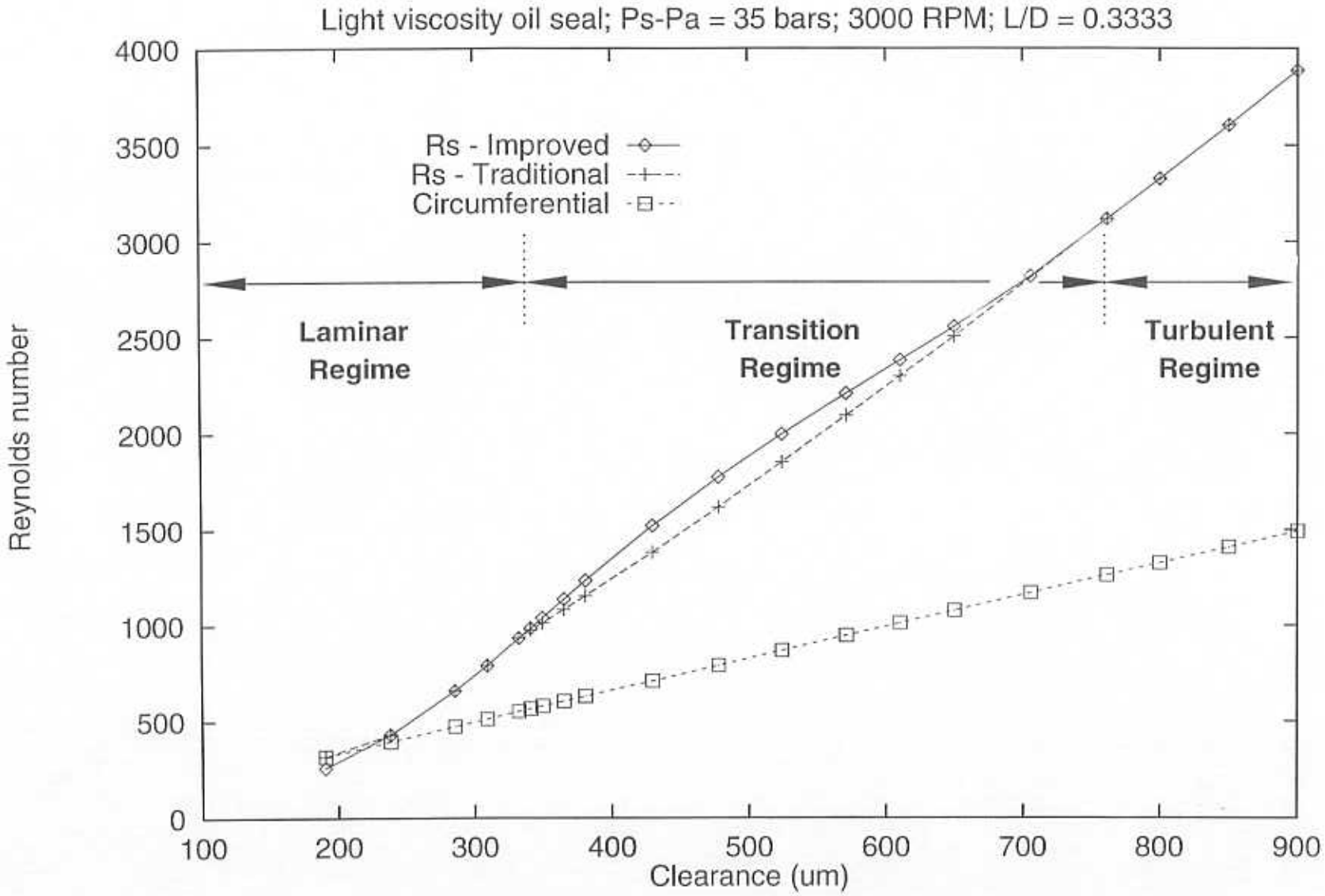

Figure 5. Flow Reynolds number (Rs) and circumferential Reynolds number vs. Operating clearance

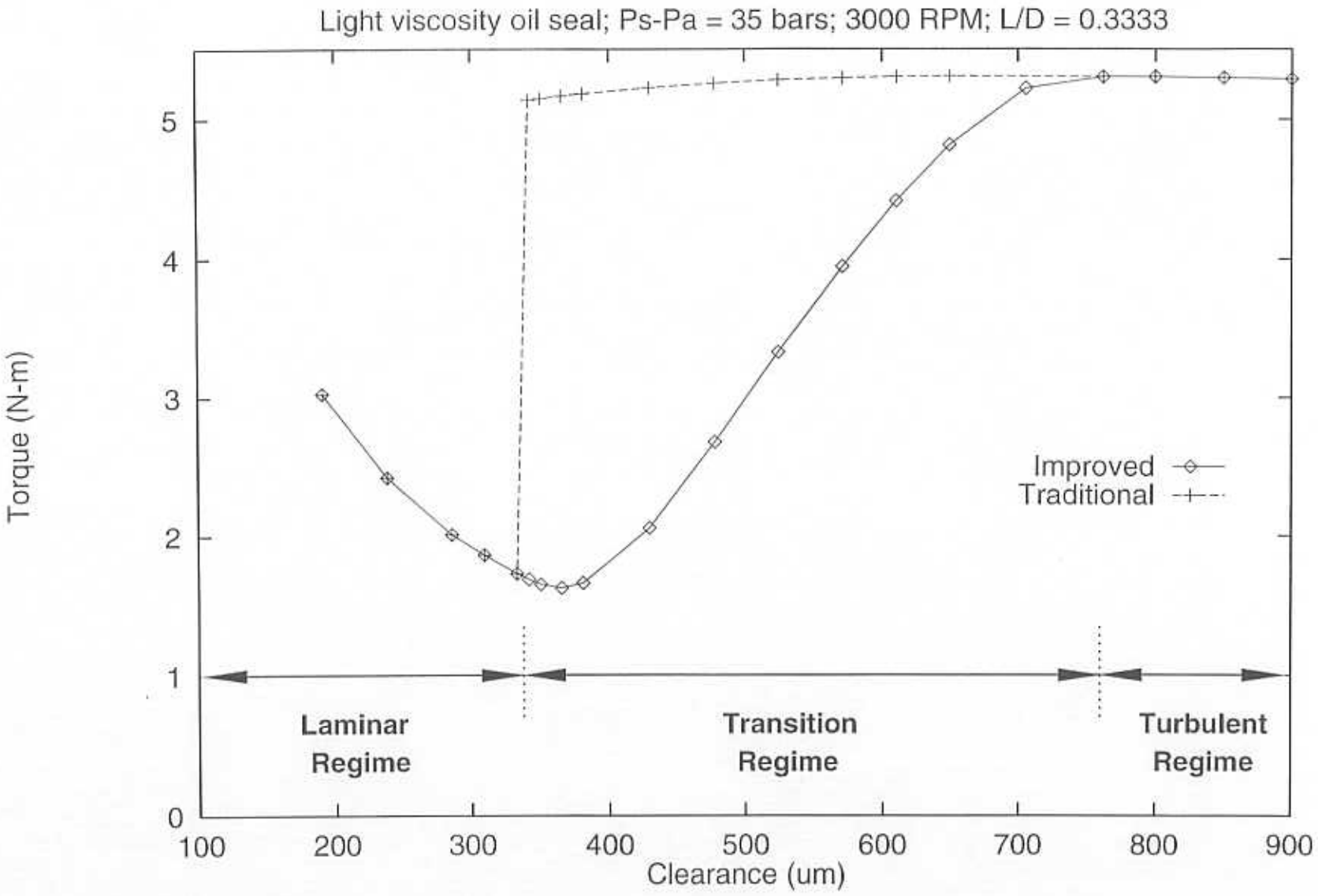

Figure 6. Drag torque vs. Operating clearance

Figures 7 through 12 depict the dynamic force coefficients as they vary with seal clearance. The graph for the direct stiffness coefficients (K_{XX}, K_{YY}), shown in Figure 7, shows that the direct stiffness continues to increase into the transition flow regime. After reaching a maximum in this zone, the direct stiffness coefficient generally decreases into the turbulent flow regime. Thus, an optimum (maximum) value for direct stiffness is obtained just after the start of the transition flow regime. The cross-coupled stiffness coefficients ($K_{XY} = -K_{YX}$) decrease from the laminar flow regime into the transition flow regime, as shown in Figure 8. After increasing in the transition regime, the cross-coupled stiffness coefficient decreases into the onset of turbulence. Figure 9 shows that the direct damping coefficients (C_{XX}, C_{YY}) reaches a minimum in the transition flow regime after decreasing from the laminar flow regime. The direct damping coefficients rise in the transition zone but decrease into the turbulent flow regime. The cross-coupled damping coefficients ($C_{XY} = -C_{YX}$), illustrated in Figure 10, generally decreases with increasing seal clearance. The improved analysis shows a less dramatic drop in the cross-coupled damping coefficient than predicted in the traditional analysis for the onset of the transition flow regime.

The direct inertia coefficients (M_{xx}, M_{yy}) depicted in Figure 11 also decrease with increasing seal clearance. From the laminar flow regime, the direct inertia is expected to decrease into the transition flow regime. After increasing slightly, the direct inertia continues decreasing into the turbulent flow regime. Figure 12 indicates that the cross-coupled inertia coefficients dramatically decrease just after the onset of the transition flow regime and remains mostly constant into the turbulent flow regime. The results suggest erratic behavior of the cross-coupled inertia; however, this force coefficient is

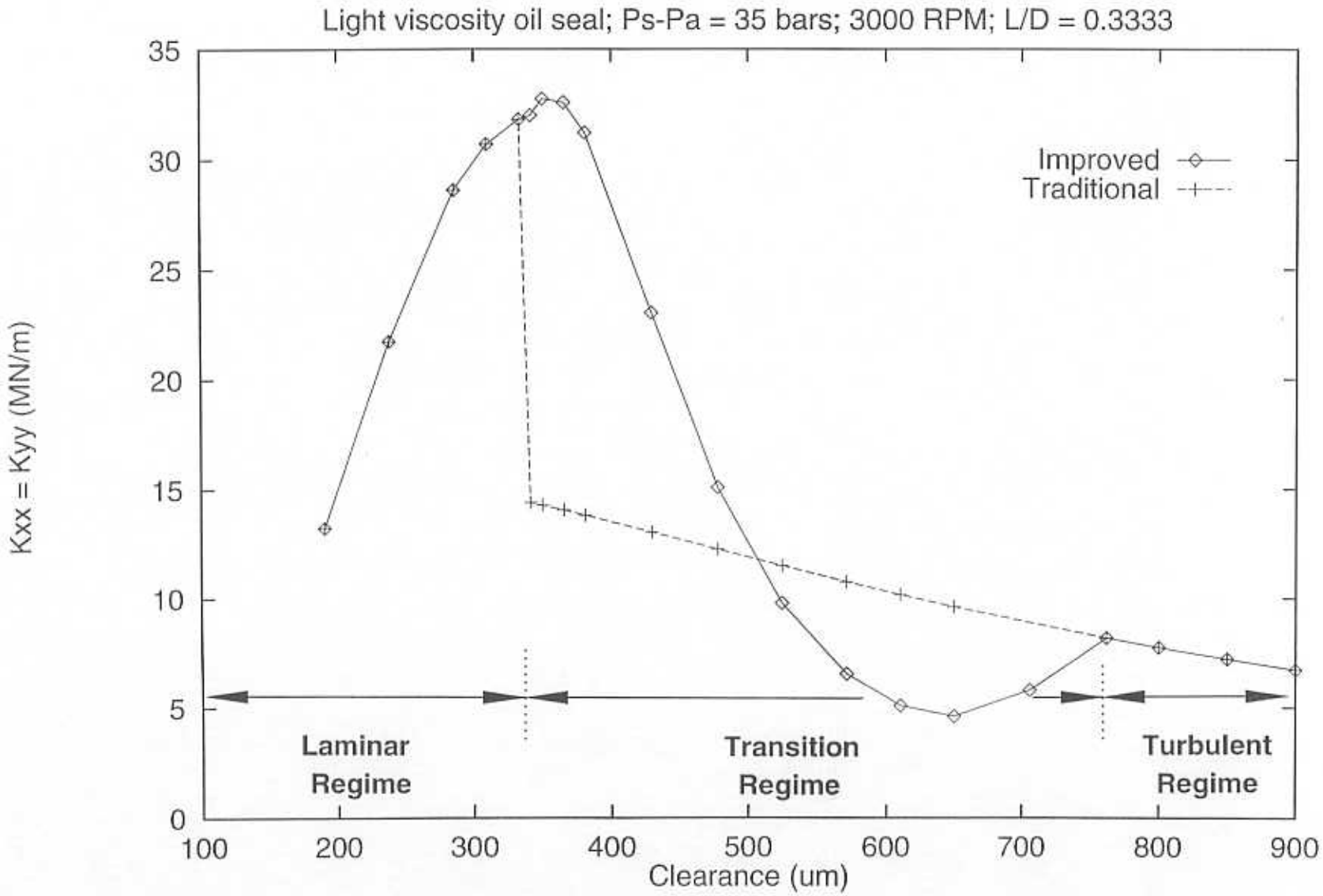

Figure 7. Direct stiffness coefficients (Kxx, Kyy) vs. Operating clearance

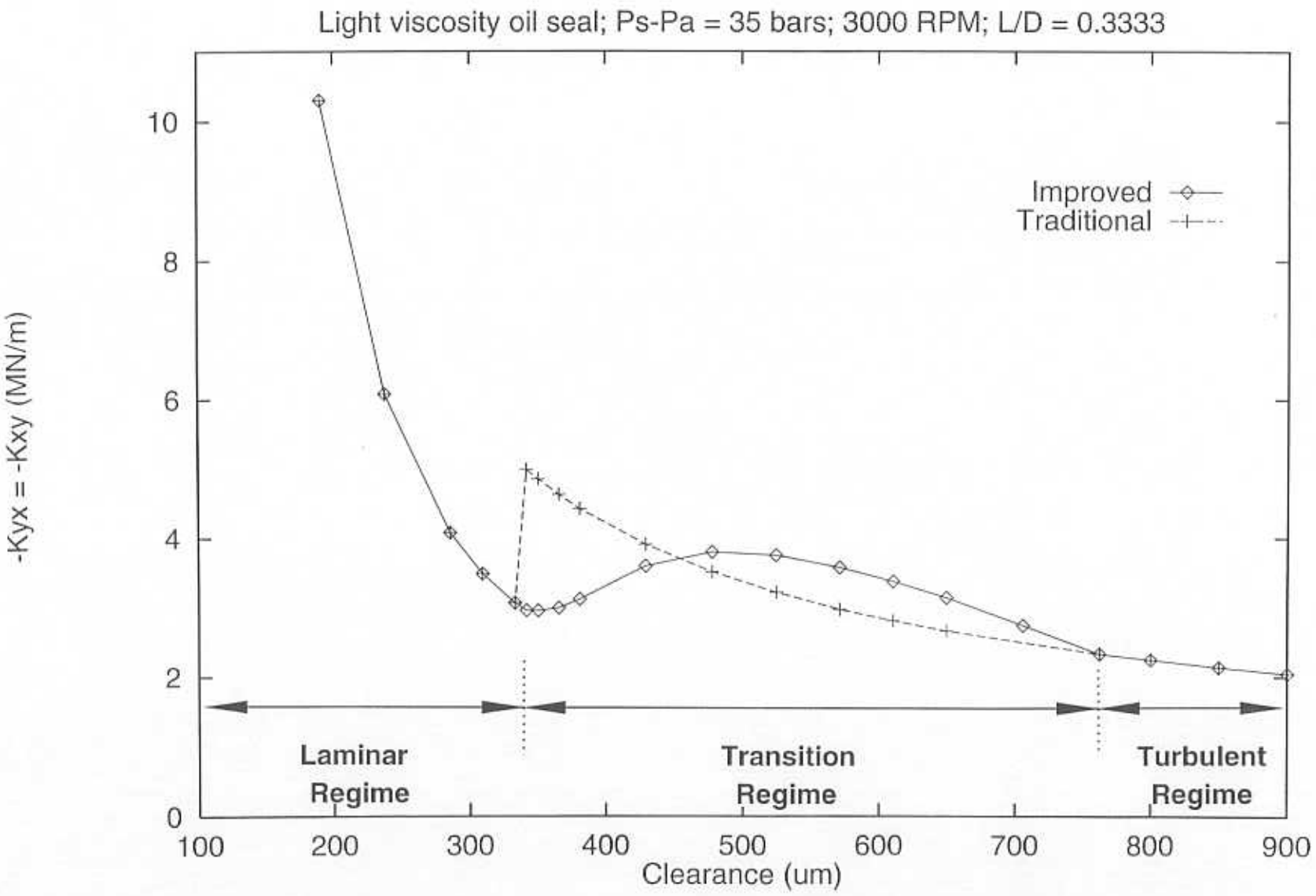

Figure 8. Cross-coupled stiffness coefficients (Kxy=-Kyx) vs. Operating clearance

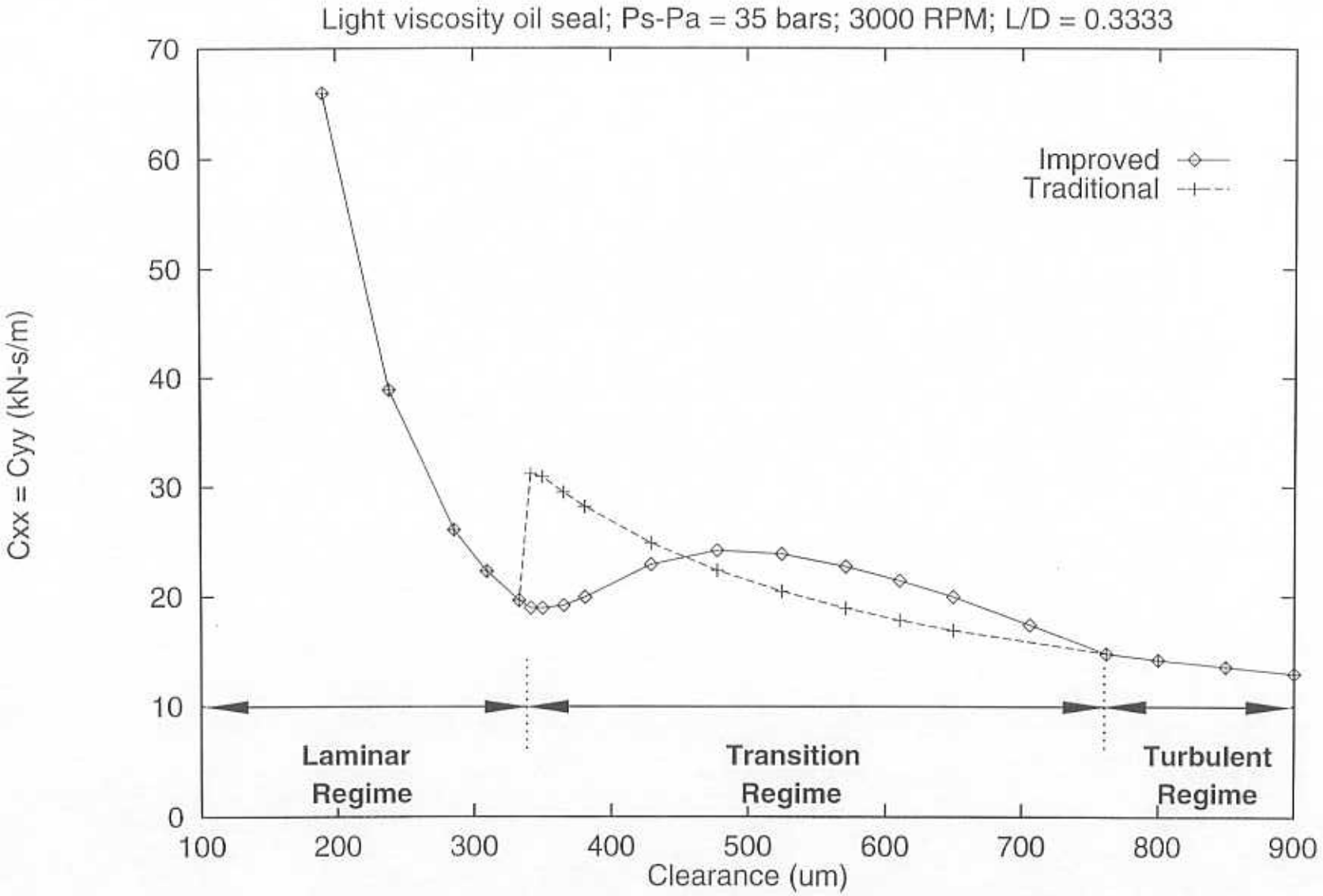

Figure 9. Direct damping coeffcients (Cxx, Cyy) vs. Operating clearance

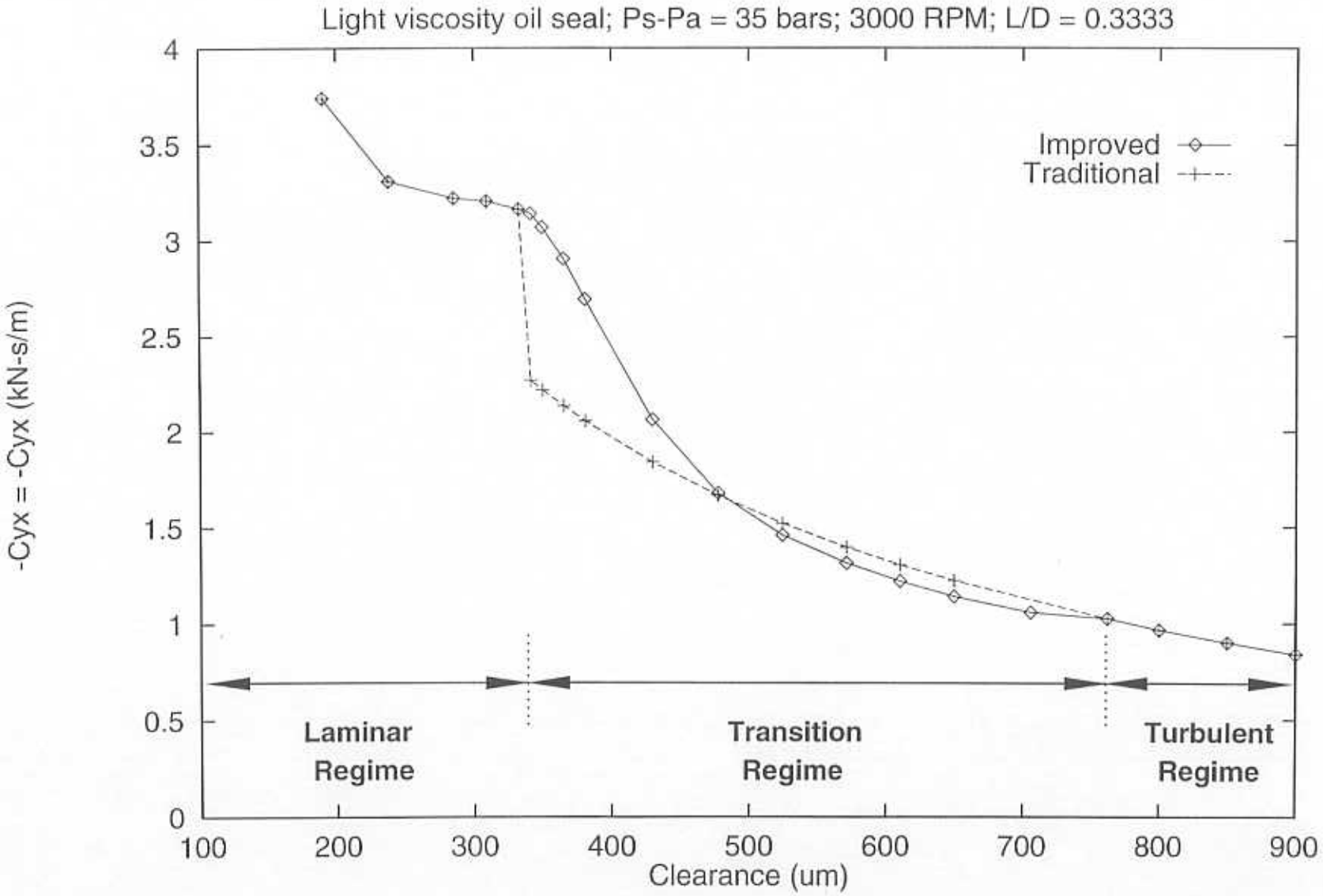

Figure 10. Cross-coupled damping coefficients (Cxy=-Cyx) vs. Operating clearance

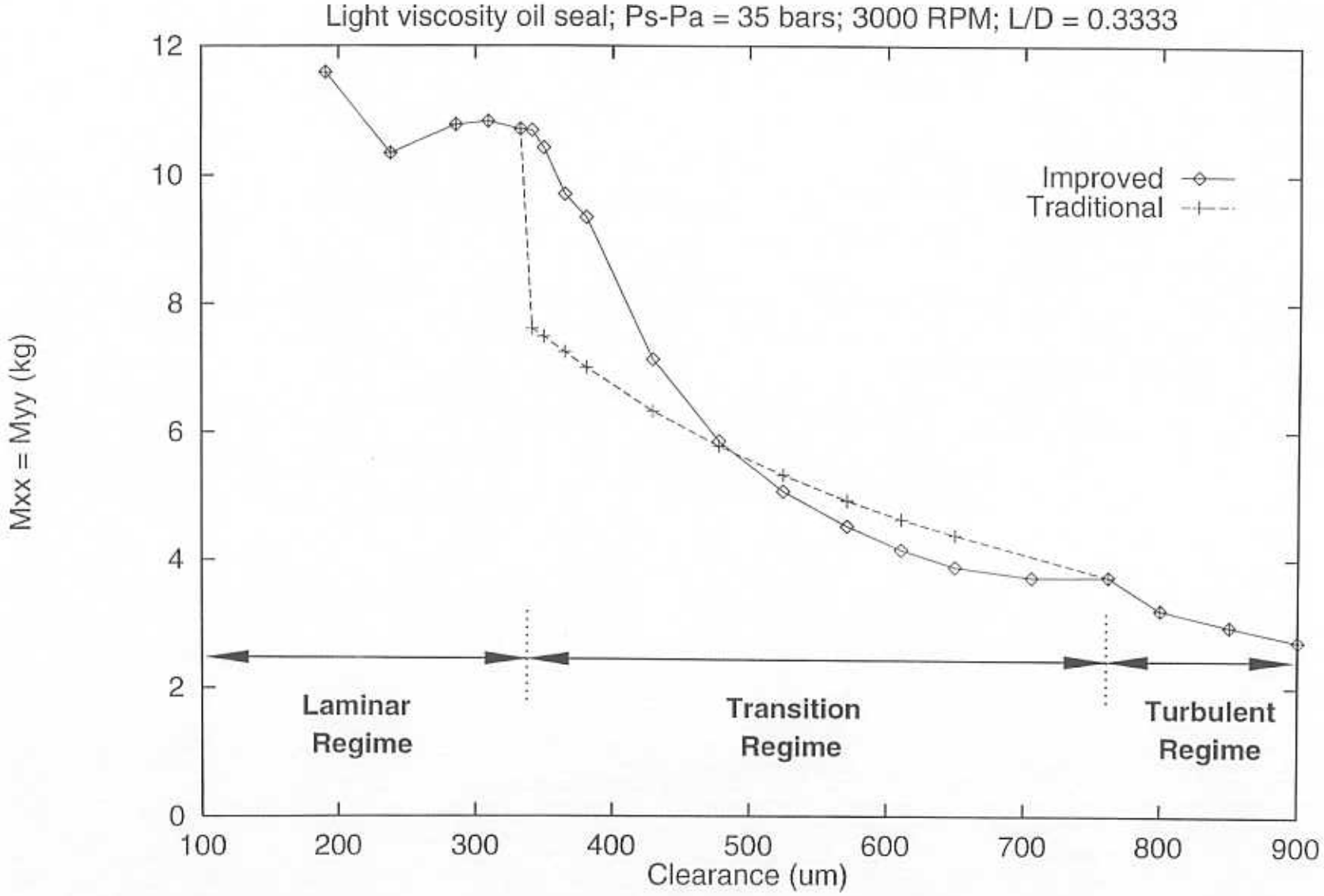

Figure 11. Direct inertia coefficients (Mxx, Myy) vs. Operating clearance

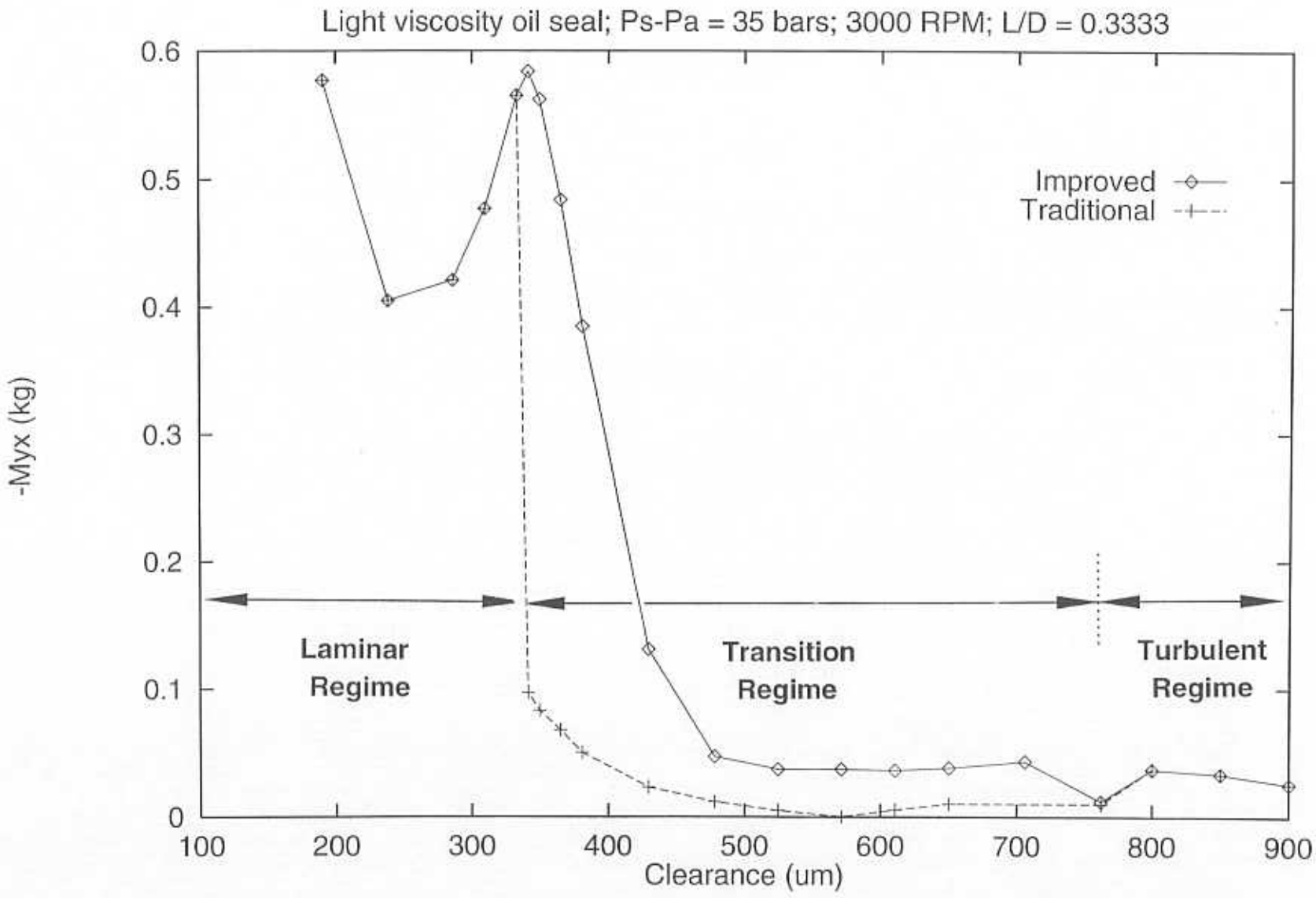

Figure 12. Cross-coupled inertia coefficients (Mxy=-Myx) vs. Operating clearance

relatively small compared with the effects from the other force coefficients. For each computation, the seal whirl frequency ratio remained constant at approximately 0.5 and did not vary between the two models. A seal whirl frequency ratio of 0.5 is a natural consequence of the inlet circumferential preswirl specified for the test cases.

A seal designed for use in the laminar flow regime may experience a large increase in direct stiffness and a decrease in cross-coupled stiffness, direct damping, and direct inertia upon entering the transition flow regime after wearing. A seal which operates in the turbulent regime after wearing may undergo a general decrease in all of the rotordynamic force coefficients.

CONCLUSIONS

Annular seals typically operate in the turbulent flow regime, because of high axial pressure gradients and large clearance to radius ratios. However, high viscosity fluids and relatively slow rotor speeds along with worn clearances typical in the petrochemical industry induce flows in the transition regime to turbulence. Traditional models for predicting force coefficients account for both laminar and turbulent flows simplifying the flow in the transition regime as fully developed turbulent flow. To provide a better physical model for the determination of rotordynamic coefficients, the equations which govern flow in annular seals are modified to include a prediction for behavior in the transition flow regime. A proposed cubic equation connecting the laminar friction factor line to turbulent friction factor lines on the Moody diagram provides a more accurate model for the friction factor within the transition flow regime. Computed predictions

show elimination of the discontinuities that exist in traditional calculations for the dynamic force coefficients. The improved analysis also indicates an optimum value for direct stiffness just after the onset on the transition flow regime.

APPENDIX

Summary of friction factors used in the seal program HSEALM:

$$f_{r,s} = \begin{cases} \dfrac{12}{R_{r,s}}, & R_{r,s} \le 1000 \\ \dfrac{12}{R_{r,s}}\left(1 - 3\xi^2 + 2\xi^3\right) + f^*_{r,s}\left(3\xi^2 - 2\xi^3\right), & 1000 < R_{r,s} < 3000 \\ f^*_{r,s}, & R_{r,s} \ge 3000 \end{cases} \qquad \textbf{(A.1)}$$

BIBLIOGRAPHY

Black, H. F., 1969, "Effects of Hydraulic Forces in Annular Pressure Seals on the Vibrations of Centrifugal Pump Rotors," *Journal of Mechanical Engineering Science*, Vol. 11, pp. 206-213.

Black, H. F. and Jenssen, D. N., 1971, "Effects of High Pressure Ring Seals on Pump Rotor Vibrations," *ASME Paper* 71-WA/FF-38.

Childs, D. W., 1983, "Dynamic Analysis of Turbulent Annular Seals Based on Hirs Lubrication Equation," *ASME Journal of Lubrication Technology*, Vol. 105, pp. 429-436.

Hirs, G. G., 1973, "A Bulk Flow Theory for Turbulence in Lubricating Films," *ASME Journal of Lubrication Technology*, 95, 2, pp. 137-146.

Nelson, C. and Nguyen, B., 1987, "Comparison of Hirs' Equation with Moody's Equation for Determining Rotordynamic Coefficients of Annular Pressure Seals," *ASME Journal of Tribology*, Vol. 109, pp. 144-148.

San Andres, L. A., 1991, "Analysis of Variable Fluid Properties, Turbulent Annular Seals," *ASME Journal of Tribology*, Vol. 113, pp. 694-702.

Shapiro, W.; Artiles, A.; Aggarwal, B.; Walowit, J.; Athavale, M.; and Przekwas, A., 1991, "Numerical, Analytical, Experimental Study of Fluid Dynamic Forces in Seals," *Mechanical Technology Incorporated Interim Report No. 1.*

Von Pragenau, G. L., 1982, "Damping Seals for Turbomachinery," *NASA TP* 1987.